

Predicting Anthropometric Body Composition Variables Using 3D Optical Imaging and Machine Learning

Gyaneshwar Agrahari^{*1}, Kiran Bist¹, Monika Pandey¹, Jacob Kapita¹, Zachary James¹, Jackson Knox¹, Steven Heymsfield², Sophia Ramirez², Peter Wolenski¹, Nadejda Drenska¹

^{*}Corresponding author: gyan.agrahari77@gmail.com

¹Louisiana State University

²Pennington Biomedical Research Center, Louisiana State University

Abstract

Accurate prediction of anthropometric body composition variables, such as Appendicular Lean Mass (ALM), Body Fat Percentage (BFP), and Bone Mineral Density (BMD), is essential for early diagnosis of several chronic diseases. Currently, researchers rely on Dual-Energy X-ray Absorptiometry (DXA) scans to measure these metrics; however, DXA scans are costly and time-consuming. This work proposes an alternative to DXA scans by applying statistical and machine learning models on biomarkers (height, volume, left calf circumference, etc) obtained from 3D optical images. The dataset consists of 847 patients and was sourced from Pennington Biomedical Research Center. Extracting patients' data in healthcare faces many technical challenges and legal restrictions. However, most supervised machine learning algorithms are inherently data-intensive, requiring a large amount of training data. To overcome these limitations, we implemented a semi-supervised model, the p -Laplacian regression model. This paper is the first to demonstrate the application of a p -Laplacian model for regression. Our p -Laplacian model yielded errors of $\sim 13\%$ for ALM, $\sim 10\%$ for BMD, and $\sim 20\%$ for BFP when the training data accounted for 10 percent of all data. Among the supervised al-

gorithms we implemented, Support Vector Regression (SVR) performed the best for ALM and BMD, yielding errors of $\sim 8\%$ for both, while Least Squares SVR performed the best for BFP with $\sim 11\%$ error when trained on 80 percent the data. Our findings position the p -Laplacian model as a promising tool for healthcare applications, particularly in a data-constrained environment.

Keywords: semi-supervised, p -Laplacian, ALM, BFP, BMD

1. Introduction

With the rise of applications in artificial intelligence in healthcare, personalized treatment and medicine have seen tremendous advances [8]. Estimating biometrics accurately is essential to gaining insights into personalized human health. Health researchers and nutritionists use several types of biometrics- metabolic (cholesterol, insulin), performance-based (speed, balance) and physiological (lean mass, body fat). Appendicular Lean Mass (ALM), Body Fat Percentage (BFP), and Bone Mineral Density (BMD) are three of the most significant physiological bio-

metrics. ALM is linked to malnutrition risk and age-related frailty, and serves as a risk factor for adverse treatment outcomes associated with metabolic syndrome (MetS) and other clinical conditions [6]. BFP is associated with obesity and cardiovascular diseases [32]. Similarly, BMD is instrumental to determining osteoporosis condition [13].

Researchers have been using DXA or Dual-energy X-ray Absorptiometry to estimate these biometrics directly. Using a scan like DXA, however, is costly, time-consuming, and inconvenient for both researchers and patients. An alternative approach is to estimate the biometrics by applying mathematical models to body measurements like height, weight, leg volume, and waist circumference. This approach involves two key steps: (1) extraction of the body measurements and (2) applying a mathematical model on these measurements. There have been developments in both these two key steps. Recent advancements now enable us to capture 2D and 3D digital images of people not only at research labs and hospitals but also at home using smartphone applications [23]. The body measurements can be extracted from these images using a computer program. Such advancements have made the extraction of the body measurements cost-effective and time-efficient. For the second key step, traditionally, statistical tools like Anthropometric body composition prediction equations have been used to make the estimations, which typically do not account for non-linear relationships [22]. In the past decade, however, machine learning algorithms have been proven to be more accurate and more efficient for estimating biometrics [16]. Models, especially the supervised algorithms, require a substantial amount of data to be trained on [1]. However, the training data

is typically acquired through imaging techniques such as DXA, which are costly to procure and operate.

In recent years, several machine learning algorithms have been developed that require less data to be trained on without significant loss of accuracy [30]. Specifically, semi-supervised algorithms, such as Semi-supervised support vector machines and graph-based label propagation have been proven efficient when training data is scarce [29]. In recent years, researchers used semi-supervised algorithm in many bioinformatics applications including predict anthropometric body compositions. Azadifar and Ahmdadi [4] used a semi-supervised learning method based on graph convolutional networks to classify and rank candidate disease genes. Their model outperformed many similar models when tested on sixteen diseases [4]. Zheng et.al[33] used a semi-supervised learning self-training algorithm to predict BMD plain hip X-ray images BMD estimation method and achieved high Pearson correlation coefficient of 0.8805.

In this paper, we will focus on such a semi-supervised algorithm - p -Laplacian based regression. We will use it alongside several supervised learning algorithms to predict the three biometrics: ALM, BFP, and BMD.

The paper is structured as follows. In Section 2, we highlight the existing literature on predicting ALM, BFP and BMD using statistical and machine learning algorithms. In Section 3, we briefly describe how the anthropometric measurements were obtained. Section 4 includes a brief data summary. In Section 5, we explain the methodology of our analysis. Section 6 briefly describes the supervised algorithms we implemented, whereas Section 7 does that for only semi-supervised algorithm - p -Laplacian

based regression - in more detail. Section 8 encompasses all the main results from our analysis. We discuss our main findings and future work in Section 9.

2. Literature Review

Previous studies such as [31, 24, 2] have shown that machine learning models are accurate in predicting ALM, BMD, or BFP. Wu, *et al.* in [31], used random forest, gradient boosting, neural network, and linear regression models to predict BMD. They found that the gradient boosting model performed the best on a dataset comprised of 1103 individual Single Nucleotide Polymorphisms (SNPs). However, when they used Genetic Risk Scores (GRS's) as input data, all models performed similarly to one another.

Shioji *et al.* in [24] used a dataset of 135 Japanese women of ages over 50 to train and predict BMD and bone loss rates using artificial neural networks [24]. The authors discovered that neural networks performed better than multiple regression approaches.

Alves, *et al.* in [2] discovered that the gender of a person influences the prediction of BFP. They used a dataset composed of both male (84) and female (79) subjects and developed various machine learning models to predict BFP on the combined dataset as well as on the datasets split up by gender. The model types used to predict BFP were random forest regression, extreme gradient boosting, decision tree, support vector regression, multi-layer perceptron (MLP) regression, and least square support vector regression (LSSVR). They observed that when using the combined dataset, the mean absolute error (MAE) range was between 3.569 and 9.859; the LSSVR achieved the best performance, and

MLP reached the worst when using the combined dataset [2]. However, the BFP error range decreased to a low of 2.756 with LSSVR and a high of 6.15 with MLP when the dataset was restricted to males only. For the females, the error ranged from 4.004 with LSSVR to 8.003 with MLP.

Marazzato, *et al.* [21] used a neural network with 1 input, 3 hidden, 2 dropout, and 1 output layers to predict ALM from 10 demographic and 43 digital anthropometric measurements acquired using a 3D optical scanner [21]. They used a dataset with 576 subjects. The results, showing small mean, absolute, and root-mean square errors, helped Marazzato *et al.* to recommend the use of neural networks to predict ALM.

Barbosa *et al.* used a dataset of 190 participants (118 women and 72 men) to predict ALM using muscle thickness measurements extracted via ultrasound [5]. They recommended using two prediction equations after observing that the developed equations produced unbiased ALM estimates that were close to the reference measurements found by the Ultrasound scanner.

There have been limited applications of semi-supervised (SSL) algorithms in predicting ALM, BMD, and BFP. Zheng *et al.*[33] used a semi-supervised learning self-training algorithm to predict BMD plain hip X-ray images BMD estimation method, and achieved a high Pearson correlation coefficient of 0.8805. Our work initiates the application of SSL algorithms in the prediction of anthropometric body composition variables. To our knowledge, this technique has not been used to predict ALM, BMD, or BFP in previous research.

3. Data Extraction

All the body measurements, here referred to as biomarkers, were gathered at the Pennington Biomedical Research Center (PBRC) facility [25]. There were 847 participants, and each participant had measurements of biomarkers such as the circumference and/or length of chest, waist, hip, arm, thigh, etc. deduced from the 3D image. The image was created from 2D images taken by one of the 3 different machines, namely (i.) the Proscanner, which uses three stationary cameras aligned vertically on a column to image a person standing on a rotating turntable, (ii.) the Styku machine, which has a similar design as the Proscanner but with a single camera, and finally (iii.) the SS20, which has 5 cameras positioned on 4 different vertical columns to capture the image [25].

The images from the machines were used to create a 3D triangular mesh with the 3D vertices representing cloud points and the area between them making a surface. Then, software created in Matlab by LSU’s Math Consultation Clinic (MC^2) group corrects any errors in the meshing [25], such as any errors in the mesh, correcting surfaces and filling any holes in the mesh.

After the mesh is corrected, it is segmented into various parts of the body which are the center, right arm, right leg, left arm, and left leg. Then each data point is taken from the segmentation which creates the dataset of body parts from each patient [25]. Out of all the measured biomarkers, we have used 44 biomarkers in this study.

4. Data Description

Pennington Biomedical Research Center in Baton Rouge, Louisiana provided the data used for this research. The collected data was utilized to predict ALM (Appendicular Lean Mass), BMD (Bone Mineral Density), and BFP (Body Fat Percentage). Additionally, influenced by the dependence of the three target values on sex, we conducted an in-depth data analysis by dividing it into three datasets: Male, Female, and Combined (the entire dataset). Using a correlation matrix, we examined the correlation of the biomarkers with the target variables (ALM, BMD, and BFP) and identified the top 10 biomarkers for each dataset.

4.1. Dataset Characteristics and Structure

The dataset contains numerical and categorical data and is stored in a widely used CSV format. The dataset’s structure includes rows representing individual participants and columns representing various measurements. Each row contains the data for a single participant. Similarly, the columns include categorical variables like gender and race and numerical variables like age, ALM, BMD, BFP, and various body measurements.

4.2. Data Cleaning

We removed participants with missing values in order to clean the data. After eliminating the rows with missing entries, we used the remaining clean data for the training and testing purposes. The cleaned data is composed of a total of 515 people and their respective 44 biomarkers. During training and testing, we excluded some of columns such as "Site", "Race" and "Gender".

Finally the dataset is composed of 3 target variables and 44 biomarkers.

4.3. Descriptive Statistics

The dataset consists of 245 males and 270 females, showing a slightly higher number of female participants. In the combined dataset, the top ten biomarkers demonstrate a strong positive correlation with ALM (over 0.9), a moderate correlation with BMD (0.7 to 0.81), and a lower correlation with BFP (0.4 to 0.6). When analyzing the data separately, most of the biomarkers showed a stronger correlation with ALM and BMD in males than in females. However, among the top ten biomarkers, Surface Area Total shows the highest correlation with ALM in both sexes.

For BFP, the correlation with the top ten biomarkers is slightly higher in females (0.6 to 0.76). In both genders, Horizontal Waists showed the strongest correlation with BFP. This high correlation is consistent with the research finding that adult women generally have higher body fat percentages than men[17].

For BMD, the Surface Area Arm is most strongly associated with males, while Height is the most influential factor in females. Biologically, testosterone in males contributes to greater BMD, while estrogen plays a crucial role in maintaining bone density in females [28]. However, after menopause, a significant drop in estrogen levels can lead to an increased risk of bone loss and osteoporosis in women.

Table 1 summarizes statistics for various physiological and demographic parameters across male, female, and combined datasets. Males display an average ALM of 21.88 kg and a BFP of 25.20%, while females show lower ALM (15.77 kg) but higher BFP (34.71%), with the com-

		Mean	Median	SD
Male	ALM (kg)	21.88	23.40	7.95
	BFP (%)	25.20	24.96	7.67
	BMD	1.07	1.10	0.19
	Age	27.33	17.00	19.59
	Height (cm)	164.33	171.20	17.80
	Weight (kg)	68.24	69.70	25.88
Female	ALM (kg)	15.77	15.50	4.24
	BFP (%)	34.71	34.90	7.37
	BMD	1.00	1.01	0.14
	Age	27.88	17.00	20.25
	Height (cm)	156.68	158.75	12.47
	Weight (kg)	60.00	58.85	18.22
Combined	ALM (kg)	18.68	17.90	6.98
	BFP (%)	30.19	30.14	8.89
	BMD	1.03	1.04	0.17
	Age	27.62	17.00	19.92
	Height (cm)	160.32	162.40	15.70
	Weight (kg)	63.92	63.20	22.55

Table 1: Summary of Statistics Related to Male, Female, and Combined

combined data reflecting intermediate values (ALM at 18.68 kg, BFP at 30.19%). Although ALM is slightly positively skewed, BFP and BMD distributions are balanced across all datasets. The data predominantly consists of younger individuals with a median age of 17, although older individuals raise the mean age to 27.62. Both height and weight show considerable variability, with high variance in the top ten biomarkers for BMD, BFP, and ALM. This variability also indicates diverse physiological measurements and notable individual differences within the sample.

5. Methodology

We tested all the models on three datasets - Male, Female, and Combined - for each target

variable: ALM, BMD, and BFP. We investigated the effects of normalizing the data using both the `StandardScaler()` and `MinMaxScaler()` classes from scikit-learn. The `StandardScaler()` outperformed `MinMaxScaler()` in our experiments, so we use the `StandardScaler()` throughout this article. To validate the models' analysis, we used *K*-Fold Cross Validation. For the semi-supervised model, we further modified the *K*-Fold cross validation to train the model on a smaller percentage of training data. In any case, we independently ran the models 10 times where in each run the data was split into *K* folds randomly.

5.1. K-Fold Cross Validation

K-fold cross-validation is a statistical method used to evaluate the performance and robustness of machine learning models. In *K*-fold cross-validation, the dataset is divided into *K* equally sized subsets or folds. The training is performed on the *K* - 1 folds and then tested on the remaining fold [19, 18]. The process of training and testing is then repeated *K* times, so that each fold is used for testing in turns. Then, the *K*-fold results are averaged to produce a single performance metric. This method is necessary because it provides a more accurate estimate of a model's performance compared to a single train-test split, because it reduces the variance associated with the random division of data. Additionally, *K*-fold cross-validation helps identify whether a model is overfitting or underfitting by making sure that every data point is used for training and validation. Thus, it improves the generalizability of the model to unseen data and aids in hyperparameter tuning and model selection [20].

5.2. Error Analysis

We used Root Mean Square Error (RMSE) in percent, given by Equation 1, to optimize our models. Our goal is to predict ALM, BFP, and BMD with the highest accuracy possible. The RMSE is expressed as a percentage for better comparison across models, target variables, and datasets.

$$\text{RMSE} = \frac{\sqrt{\frac{1}{N} \sum_{i=1}^N (\hat{y}_i - y_i)^2}}{\sqrt{\frac{1}{N} \sum_{i=1}^N y_i^2}} \times 100 \quad (1)$$

where,

y_i = True value of ALM, BFP, or BMD,

\hat{y}_i = Predicted value of ALM, BFP, or BMD,

and

N = Number of patients in the testing set.

Each model was implemented 10 times where each run was implemented with *K*-cross validation. The average RMSE for the model was calculated by the taking average over all runs and *K*-folds. For example, if $K = 5$, the average was taken over 50.

6. Supervised Learning Algorithms

In this section, we present an overview of the supervised algorithms we implemented. For these models, we use the standard 80-20 split with *K*-fold cross-validation for $K = 5$, hence hereon we will refer to it as 5-fold cross validation. That is, 20% of the data is used for testing in each fold. In this section, we briefly describe the supervised models we use. We discuss our results for these models in the Results and Analysis section.

6.1. Linear and Polynomial Regression Models

Linear Regression (LR) and Polynomial Regression (PR) are widely used techniques in machine learning. However, they are susceptible to underfitting or overfitting and sensitive to outliers [18]. To improve their efficiency, researchers have developed variations of LR and PR [27]. In this study, we implemented three such variations—Lasso, Ridge, and Bayesian—along with traditional LR and PR. Due to time complexity, we implemented PR of degree 2 and degree 3 only.

6.2. Support Vector Regression Models

Support Vector Regression (SVR) is an extension of regression models to higher dimensions with additional features. SVR applies a kernel function that maps the raw data into higher dimensions. The model then tries to fit the transformed data within an ϵ margin of a hyperplane. There are several choices for the kernel function [3]. In our experiments, the Linear kernel outperforms other kernel functions for SVR. The penalty parameter C allows us to choose the trade-off between the error and over-fitting.

We applied a variant of SVR called Least Square SVR (LSSVR) with a radial basis function (RBF) kernel function. LSSVR solves a set of linear equations instead of quadratic programming like in SVR [26]. The parameter γ in LSSVR decides how influential one data point is. If γ is low, the kernel output is close to 1 for most data points, leading to under-fitting.

For SVR, we varied the values of ϵ and C whereas for LSSVR, we varied the values of C and γ .

6.3. Random Forest and Extreme Gradient Boosting Models

The Random Forest (RF) model is an ensemble learning method that averages predictions from multiple decision trees for classification and regression problems. The decision trees are trained independently of each other on random subsets of the data [14]. In the Extreme Gradient Boosting (XGBoost) model, the decision trees are added sequentially, where each new tree corrects the residual error of its predecessor. The model uses gradient descent to minimize loss. We fine-tuned the number of trees and maximum depth of a tree for both RF and XGBoost to determine which combination of these parameters minimizes RMSE [7].

6.4. Neural Network (NN)

Neural networks mimic the way neurons in the human brain function. They are designed to model and understand patterns in data by adjusting weights and biases through training [15]. The effectiveness of the model is indicated by a loss function. There are various types of neural networks suited for specific tasks. In this study, we focus on regression and have chosen a multi-layer perceptron (MLP). For the MLP, we experimented with up to four hidden layers, each associated with an activation function. The most optimal batch size was 16. We selected ReLU as the activation function for all layers. Among the optimizers tested (Adam, AdamW, RMSE-prop, and SGD), Adam yielded the best performance. MSE (Mean Squared Error) and RMSE (Root Mean Squared Error) were the loss functions used in the experiments.

7. Semi-Supervised Learning Algorithms

Semi-supervised learning is a category of machine learning algorithms that combines the utilities of unsupervised learning and supervised learning algorithms. Supervised algorithms construct a classifier or a regressor by training the dataset to find associations between the input values and the target. Such algorithms then leverage these associations to predict the output value for previously unseen inputs [19]. In an unsupervised algorithm, inputs are assigned to clusters based on feature similarity, ensuring that inputs with similar characteristics are grouped. In a semi-supervised algorithm, the relationship between labeled (training) and unlabeled (testing) data is utilized to improve the learning process [19]. A semi-supervised algorithm is useful when extracting labeled data is either computationally or financially expensive. Semi-supervised algorithms have traditionally been applied to classification tasks, as their design is often tailored specifically for classification and does not readily extend to regression problems. The class of semi-supervised learning methods known as graph-based methods can be extended to regression problems [29]. Zhu [34] is one of the first researchers to introduce graph-based semi-supervised algorithms in their thesis. We implemented a version of a graph-based method, called p -Laplacian regression introduced by Calder and Drenska in [10]. In this section, we will elucidate the underlying concepts of their model. For the sake of simplicity, we will explain the model for predicting ALM of the patients. The same procedure works for BFP and BMD. In the following discussion, by labeled vertex, we refer to a patient whose ALM value the

algorithm remembers. Such vertices are in the training set for the algorithm.

We discuss this graph-based method from [10] in two steps: (1) Graph Construction and (2) The Tug-of-War equation.

7.1. Graph Construction

We follow the standard notation and terminology for the graph. Let G be our graph with n vertices where n is the total number of patients in the dataset. Let $\mathcal{X} = \{x_1, x_2, \dots, x_n\}$ be the set of vectors in \mathbb{R}^{44} . Each x_i represents a vertex in G . Each entry in x_i is a measurement of one of the biomarkers of the patient the vertex represents. The x_i 's are first normalized using z -score normalizer. We connect two vertices x and y with an edge only when they are within the threshold of the similarity we define below. For a pair of vertices x and y , we define the Euclidean distance, $d(x, y) = \|x - y\|$ in \mathbb{R}^{44} . Intuitively, for the pair of vertices x and y , the greater the value of $d(x, y)$ is, the less similar the patients corresponding to x and y are. Therefore, we need a nonnegative decreasing function η to define the edge weight, w_{xy} .

$$w_{xy} = \eta\left(\frac{d(x, y)}{\epsilon}\right) \quad (2)$$

where $\epsilon > 0$ is a free parameter.

Equation 2 implies $w_{xy} = w_{yx}$. Therefore, G is an undirected graph. As used in [9], we chose $\eta(t) = e^{-t^2}$ as our nonnegative decreasing function. The nondecreasing function allows us to connect nodes with nodes. Furthermore, this choice ensures the values of w_{xy} lie strictly between 0 and 1. For computational efficiency, we construct a k -nearest neighbors (k -NN) graph, where each vertex has k neighbors. We follow the method described by Calder and Trillos in

[11] to construct a k -NN graph. We denote the open neighborhood of a vertex x as N_x . Theoretically, this algorithm of constructing a k -NN works even when G is not connected, provided that each connected component of G has at least one labeled vertex. However, for the computer simulations to run, G must be connected. The primary hypothesis underlying the construction of a similarity-based graph is that individuals with similar measurements of their biomarkers have their ALM within a small margin. We estimate the ALM value of a vertex x by using the ALM values of the rest of the vertices in G . Vertices in the neighborhood of x in G have a higher influence on its ALM. The influence of the vertices declines as we move farther from x in G .

7.2. Tug-of-War Equation

Like supervised algorithms, p -Laplacian-based regression needs a training set and a testing set. We divide the vertex set, \mathcal{X} into two subsets: Γ and $\mathcal{X}\setminus\Gamma$. For vertices in Γ , we remember the values of the ALM for the corresponding patients, which makes Γ our training set. Similarly, for vertices in $\mathcal{X}\setminus\Gamma$, we temporarily forget the values of the corresponding ALM which makes the set $\mathcal{X}\setminus\Gamma$ our testing set. Let $g : \Gamma \rightarrow \mathbb{R}$ be the true value of ALM for vertices in Γ and $u : \mathcal{X} \rightarrow \mathbb{R}$ be our estimated value of ALM for vertices in \mathcal{X} . Clearly, u and g are identical in Γ .

To estimate the value of ALM for the vertices in $\mathcal{X}\setminus\Gamma$, we solve the Game-Theoretic p -Laplacian for the function u on the set $\mathcal{X}\setminus\Gamma$. Hence, the following set of equations describes our system.

$$\begin{cases} \mathcal{L}_p u(x) = 0 & \text{if } x \in \mathcal{X}\setminus\Gamma \\ u(x) = g(x) & \text{if } x \in \Gamma \end{cases} \quad (3)$$

In Equation 3, p is in $[2, \infty)$. To solve, $\mathcal{L}_p u(x) = 0$, we utilize the Dynamic Programming Principle (DPP) described in [10]. DPP can be represented by the following equation:

$$u(x) = \frac{\alpha}{d_x} \sum_{y \in N_x} w_{xy} u(y) + \frac{1-\alpha}{2} \left(\min_{N_x} u + \max_{N_x} u \right) \quad (4)$$

where, $\alpha = \frac{1}{p-1}$ and $d_x = \sum_y w_{xy}$ is the degree of vertex x .

Equation 4 arises from a stochastic two-player tug-of-war game. The details of the procedure can be found in [10].

In Equation 4, we observe when p is 2, α is 1, which results in the elimination of the terms associated with the minimum and maximum values of u . Consequently, the model relies exclusively on the random walk. For higher values of p , the contribution of the summation term diminishes. Moreover, as p becomes larger, the factor $\frac{1-\alpha}{2}$ gets closer to $\frac{1}{2}$.

We use a Python package *GraphLearning* from [9] to predict ALM. The algorithm first computes the weight matrix. The array *X_combined* stores the measurements of the 44 biomarkers for each patient. For each pair of vertices x_i and x_j in *X_combined*, the matrix *W* stores the weight $w_{x_i x_j}$. The function *gl.graph* then creates a k -NN graph from *W*.

```
W = gl.weightmatrix.knn(X_combined, k)
G = gl.graph(W)
```

Now, the algorithm runs the p -Laplacian based regression. Specifically, the function *G.plaplace* computes *yhat*, the predicted value of ALM based on the true values of ALM, *y_combined* of the training set. Clearly, *yhat*, and *y_combined*, are equal for the vertices in the training set.

```
yhat = G.plaplace(np.where(train_mask)[0],
```

`y_combined[train_mask], p)`

In Section 8.5, we discuss our results on p -Laplacian based regression.

8. Results And Analysis

In this section, we present our results for both supervised and semi-supervised algorithms. The RMSEs in this section are expressed as a percentage (see Equation 1). The figures of heatmaps and line plots include nine subplots in a grid system. The columns and rows represent the datasets and the target variables respectively.

8.1. Polynomial Regression

Polynomial regression models (Traditional, Lasso, Ridge, and Bayesian Ridge) are compared across polynomial degrees (1, 2, and 3) and datasets. A key issue with traditional regression is its tendency to suffer from high variance, which increases as the polynomial degree increases. Regularization methods, such as Ridge and Bayesian Ridge, mitigate this variance to some extent, but overall, increasing the polynomial degree generally leads to higher errors.

As Figure 11 exhibits, in the case of ALM Bayesian Ridge and Ridge Regression consistently achieve lower RMSEs (8–10 for degree 1, 10–15 for degree 2 and 15–20 for degree 3) across datasets. Traditional Regression shows higher variability, particularly for Female with RMSEs exceeding 40–50 for higher-degree models.

Similarly, Figure 12d demonstrates Bayesian Ridge and Ridge Regression outperform the Traditional one for BFP, with RMSE between 8–20 across degrees. In contrast, Traditional Regression shows significant variability, especially for

degree 3, where RMSEs exceed 40–60 for Female (Figure (12)).

Finally, Bayesian Ridge (See Figure 12) maintains the lowest RMSEs for BMD (8–20 across degrees) compared to other methods. Traditional regression struggles with variability, particularly for Male and Female, with RMSEs reaching 60–70 for degree 3.

Bayesian Ridge remains the most reliable method in all data sets and the degrees (Figure (13)).

8.2. SVR and LSSVR

For SVR with linear kernel, we optimize the regularization parameter, C , and the margin tolerance, ϵ , for predicting BMD, BFP, and ALM.

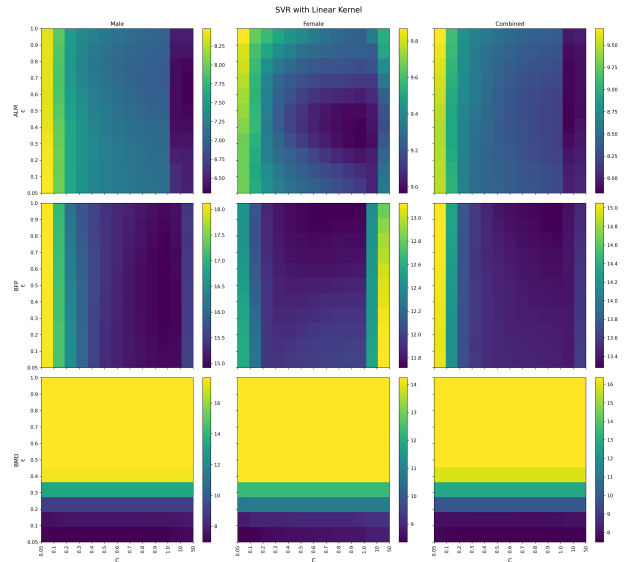


Figure 1: Heatmap of RMSEs (in %) for SVR with parameters C and ϵ

As shown in Figure 1, SVR, at its best, yields error between 6% and 9% for ALM and BMD across all datasets, with RMSE values ranging between 6% and 9%. The models performs better for Male and Combined while predicting

these two biometrics. For these two biometrics, the model performs better for Male and Combined than for Female. The model achieves optimal performance at higher values of C and ϵ for Male ALM and Combined ALM compared to Female ALM. When predicting BMD, the model optimizes at $\epsilon = 0.05$ and C in $[0, 1]$ yielding between 6-9% for all datasets. Like the regression models, SVR performs poorly for BFP specially, for Male yielding errors close to 15%.

The heatmap in Figure 2 demonstrates the performance of LS-SVR with an RBF kernel across ALM, BFP, and BMD datasets for varying values of C (regularization) and γ (kernel parameter).

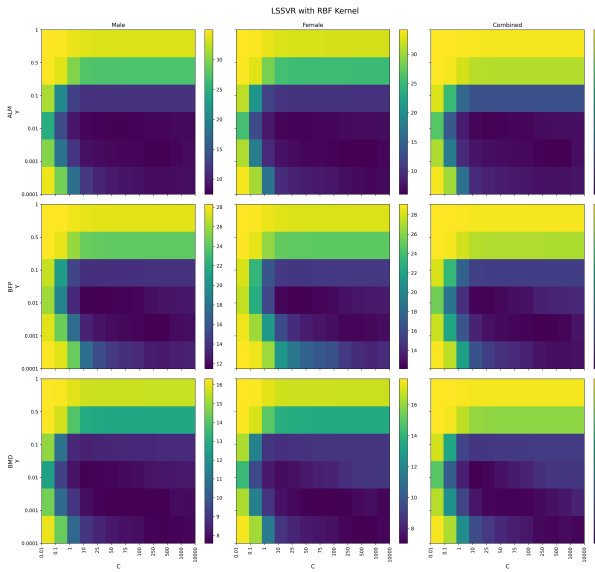


Figure 2: Heatmap of RMSEs (in %) for LSSVR with parameters C and γ

For ALM, the best performance was observed with C in the range of 500 to 1000 and $\gamma = 0.001$ achieving RMSE values between 6 % and 8 % across all datasets. For BFP, the optimal results were obtained with C in the range of 25 to 250 and γ between 0.001 and 0.01, yielding RMSE values between 11 % and 13 %. For BMD, the best-performing region had C values from 10 to

250 and γ between 0.001 and 0.01, with RMSE values ranging from 7% to 8%. These trends suggest that lower γ values combined with higher C values provide better accuracy for ALM and BMD, while BFP benefits from moderate γ and smaller C values.

8.3. Random Forest and XGBoost

For RF and XGBoost models, we varied the number of decision trees, n , and their maximum depth, d .

For RF, n and d were between 2 and 50.

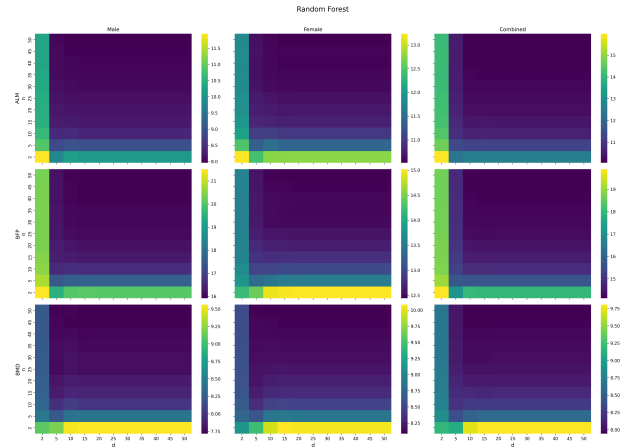


Figure 3: Heatmap of RMSEs (in %) for RF with parameters n and d

As we see in Figure 3, RF performs the best for BMD and the worst for BFP. For BMD, the RMSE for Male, Female, and Combined are 7.72% ($n = 45, d = 15$), 8.09% ($n = 50, d = 20$) and 7.94% ($n = 50, d = 10$), respectively. For ALM, RF achieves the lowest RMSEs within the range of 7 to 11 percent for all the datasets. The model performs the worst for Male BFP as the lowest RMSE for all n and d it yields is 15.92%. As demonstrated by Figure 3, the RMSE stays relatively constant for all datasets and target variables when $n \geq 25$ and $d \geq 15$,

Similar to RF, the RMSE of XGBoost exhibits

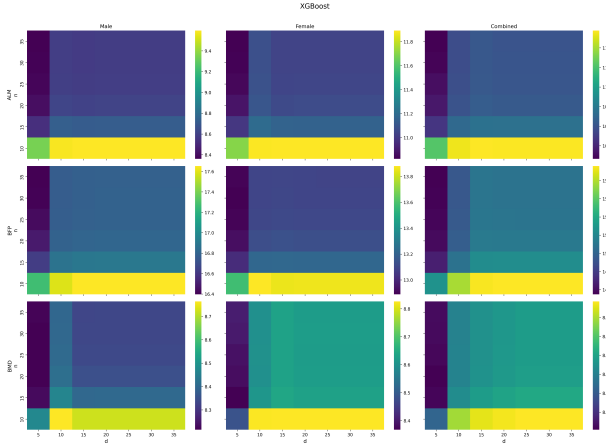


Figure 4: Heatmap of RMSEs (in %) for XGBoost with parameters n and d

minimal variation once n and d exceed a certain threshold. We tested the model for the values of n and d between 5 and 35. The model’s run time is exceptionally high for larger values of the parameters.

The model performs the best for BMD by yielding errors between 8 and 9 percent for each dataset. The RMSE for BMD for Male, Female and Combined are 8.22 % ($n = 20, d = 6$), 8.37% ($n = 15, d = 5$), and 8.31% ($n = 20, d = 5$) respectively. Like RF and the other models, its performance is the worst for BFP. In all three datasets and target variables, the model yields the highest lower limit error of 16.4 % for Male BFP. The model’s performance is similar to RF for ALM with RMSE ranging between 8-12%. As Figure 4 demonstrates, the most optimal d for XGBoost is 5 for all datasets and target variables. RMSE only increases when $d > 5$.

8.4. Neural Network

As explained in Section 6.4, we experimented with multiple activation functions, batch sizes, and optimizers. Here, we show how our neural network performed for different number of

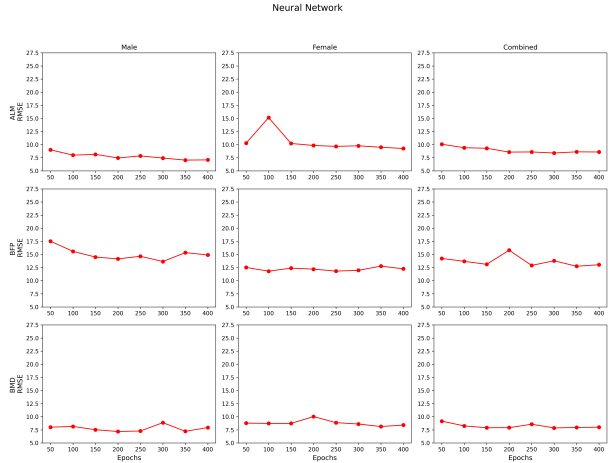


Figure 5: RMSE of Neural Network vs Number of Epochs

epochs. For Combined, as training epochs increase, RMSE for ALM, BFP, and BMD predictions drops. At 50 epochs, RMSE is higher for all three, but it stabilizes around 8.8 for ALM, 13.5 for BFP, and 8.0 for BMD at 400 epochs. This shows the model’s accuracy improves with more training, leading to better predictions.

For Female, ALM’s RMSE drops from 10.5 to 9.0 as epochs increase from 50 to 400. BFP’s RMSE improves significantly, falling from 15.0 to 13.0. BMD’s RMSE reduces from 9.0 to 8.0. More training epochs boost accuracy for all metrics in female data.

In Male, ALM’s RMSE decreases from 9.5 to 7.5 with more epochs. BFP starts high at 17.0 but drops to 14.0. BMD’s RMSE falls from 9.0 to 7.5 as the number of epochs increases. More epochs lead to better performance, especially for ALM and BFP predictions.

Overall, RMSEs consistently decrease with more epochs, showing improved predictive accuracy. This trend is more pronounced in male data.

8.5. p -Laplacian based Regression

We tested the p -Laplacian based regression under two schemes and training-testing ratios. As described in Section 7, the model is implemented on a graph where the nodes are the patients and the edges are constructed based on the similarity between the patients. We constructed the graph using two methods. In the first method, we used all 44 biomarkers to define similarity and then construct the graph. In the second method, we used the top ten biomarkers listed in Tables 4, 5, and 6 for each target variable and dataset. The idea behind this is to see if using fewer and more significant biomarkers only improves the model’s performance. We call the first method p -Laplacian-1 and the second method p -Laplacian-2. Like the supervised models, p -Laplacian-1 and p -Laplacian-2 are first implemented with K -cross validation for $K = 5$. To test the model’s performance when trained on a smaller percentage of training data, we modified the K -fold cross-validation slightly. We used one fold as our training set and the other four as our testing set. We tested both versions of the model using the modified K -fold cross-validation for $K = 2, 3, 4, 5, 10$, and 20 with training testing ratios 50-50, 33-67, 25-75, 20-80, 10-90, and 5-95, respectively.

In the following discussion, we represent the percentage of training data as Training %. We vary two parameters: p (see the description of Equation 4) and k (the number of neighbors every node has in the graph). For optimization, we implemented p -Laplacian-1 and p -Laplacian-2 for different combinations of p and k for a fixed Training %. For both models, the optimal p is at most 10 and the optimal k is at most 60. Figure 6 demonstrates how the lowest RMSE p -Laplacian-1 and p -Laplacian-2 yielded changes

with Training %. The RMSEs of both models increase as the Training % decreases. This phenomenon is not unusual. Calder and Drenska [10], showed for a random geometric graph like k -NN graph the accuracy of the p -Laplacian-based algorithm can decline with label rate which is equivalent to Training %. There is a relatively steep increase in the models’ RMSE when the Training % is reduced from 10 to 5 across all target variables and datasets. Among the target variables, they both perform the best for BMD. The yielded RMSE is less than 10.2% for all datasets when the Training % is less than or equal to 10. The RMSEs of both models follow similar trajectories for BMD. For Male ALM and Female ALM, p -Laplacian-2 does slightly better than p -Laplacian-1; however, for Combined ALM, it yields higher RMSEs than p -Laplacian-1 when Training % is at least 10. Like the supervised models, p -Laplacian-1 and p -Laplacian-2 perform poorly on estimating BFP, especially for Male and Combined. p -Laplacian-1 outperforms p -Laplacian-2 by a huge margin when estimating BFP for these two datasets. Both p -Laplacian-1 and p -Laplacian-2 perform well for BMD yielding errors below 10% for all the datasets even when they are trained on only 10 percent of the the data. The errors are slightly above 10% when Training % is reduced to 5%.

Figure 7 and Figure 8 demonstrate how the optimal parameters p and k change for p -Laplacian-1 and p -Laplacian-2, respectively with the Training %. As illustrated by Figure 7, when Training % is 10 or 5, the optimal p values for p -Laplacian-1 and p -Laplacian-2 jump above 2 for ALM and BMD. In the case of BFP, this happens for p -Laplacian-1 but not for p -Laplacian-2. Calder *et al.* [12] proved at low label rates, (equivalent to Training%) a 2-Laplacian algorithm (when

$p = 2$) becomes degenerate which implies it fails to predict the target variable with high accuracy. Another observation is that p -Laplacian-1 is optimized at much higher p values when compared to p -Laplacian-2. We did not find any evidence on why p -Laplacian-2 acts as an anomaly for BFP. One reason could be that weakly correlated biomarkers with the target variables make the convergence of the RMSEs slower. Further investigation is required to substantiate this hypothesis.

Figure 8 demonstrates the optimal k values for both p -Laplacian models. There is no obvious pattern to distinguish between the optimal k values of p -Laplacian 1 and p -Laplacian-2.

Since p can approach infinity, it is natural to investigate the asymptotic behavior of p -Laplacian based regression. Equation 4 predicts that the RMSE of a p -Laplacian based regression should converge for larger values of p . To verify this prediction, we implemented p -Laplacian-1 and p -Laplacian-2 for larger values of p by fixing $k = 10, 30$, and 50 . Figure 9 and Figure 10 demonstrate the asymptotic behavior of RMSEs of p -Laplacian-1 and p -Laplacian-2 respectively when p approaches infinity. For demonstration, Training % is fixed at 20%; however, similar results are achieved for other values of Training %. As Figure 9 and Figure 10 demonstrate, the RMSEs converge as p gets larger.

9. Discussion

There are two main objectives this article. The first is to test if ALM, BFP, and BMD can be predicted by applying supervised and semi-supervised algorithms on biomarkers' measurements obtained by the procedure described in

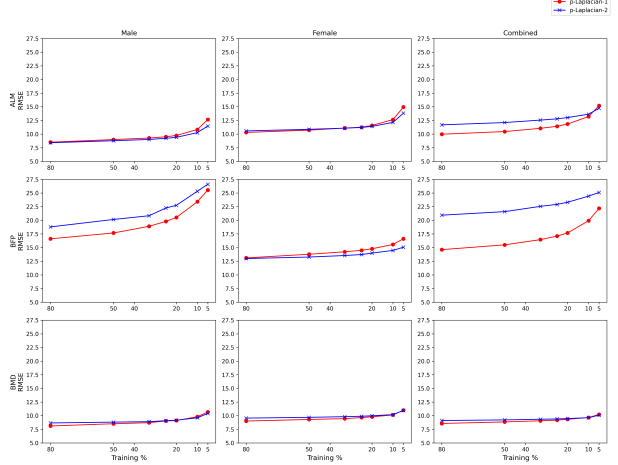


Figure 6: RMSEs (in %) vs Training % of p -Laplacian-1 and p -Laplacian-2 across the target variables and datasets

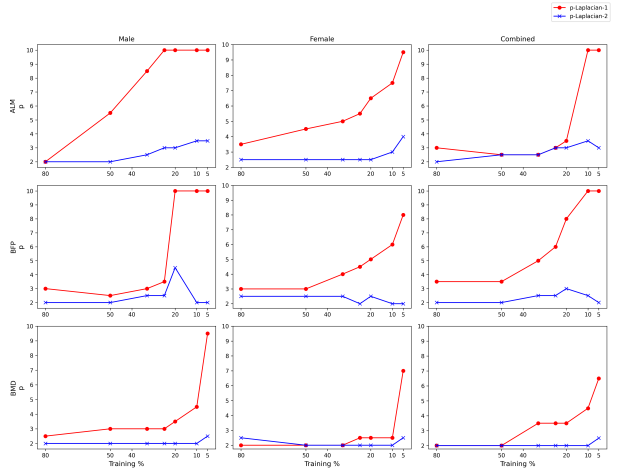


Figure 7: Optimal p vs Training % of p -Laplacian-1 and p -Laplacian-2 across target variables and datasets

Section 3. We used six different supervised algorithms namely-Linear/Polynomial Regression, SVR, LSSVR, Random Forest, XGBoost and Neural Network. The second objective is to see if we can reduce the data we need to train a model to predict these three quantities. To achieve this, we used p -Laplacian based regression, a semi-supervised algorithm.

The supervised models demonstrated signifi-

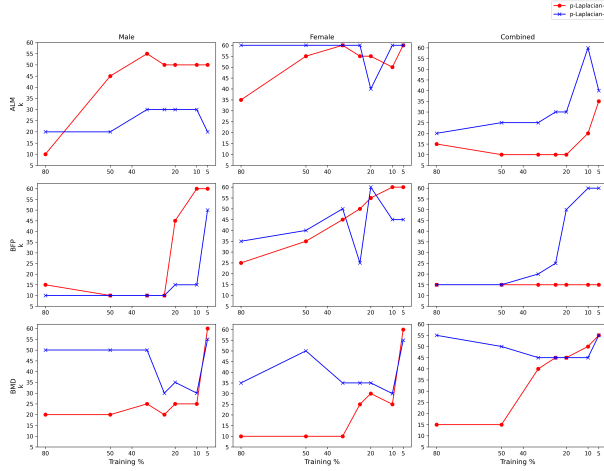


Figure 8: Optimal k vs Training % of p -Laplacian-1 and p -Laplacian-2 across target variables and datasets

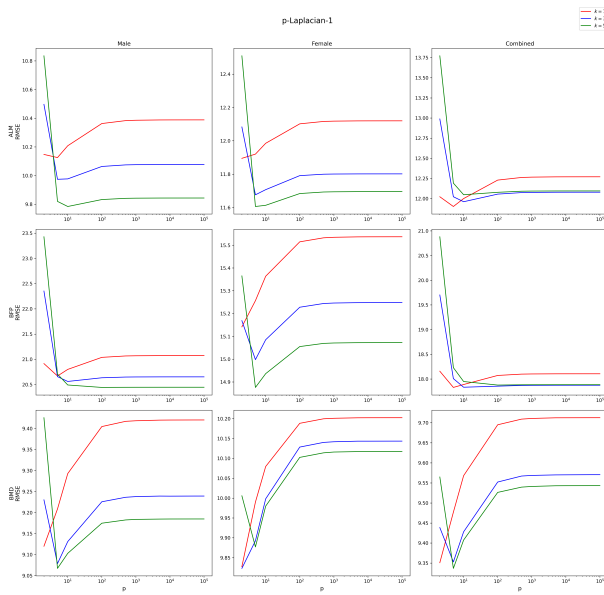


Figure 9: Asymptotic behavior of p -Laplacian-1 as $p \rightarrow \infty$ for $k = 10, 30$, and 50

cantly higher accuracy for ALM and BMD compared to BFP. The BFP predictions for Female were on average better than those for Male and Combined. One of the reasons behind models' poor performance on predicting BFP could be its relatively low correlations with the biomarkers. The SVR and LSSVR models are the most

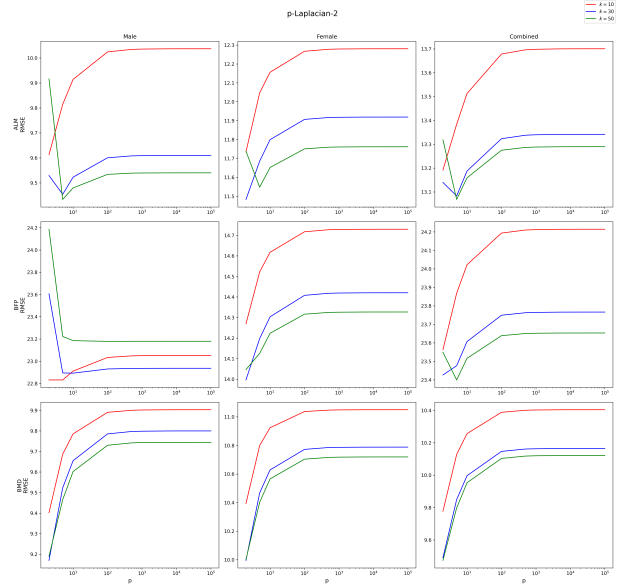


Figure 10: Asymptotic behavior of p -Laplacian-2 as $p \rightarrow \infty$ for $k = 10, 30$, and 50

accurate models for all target variables across all datasets. Here is the summary of the best performing supervised models for the target variables across all datasets with their respective RMSEs.

	ALM		BFP		BMD	
Male	SVR	6.30	LSSVR	11.47	SVR	6.97
Female	LSSVR	6.03	SVR	11.72	LSSVR	7.05
Combined	SVR	7.83	LSSVR	10.99	SVR	7.48

Table 2: Summary of the best performing Supervised Models for the Target variables with respective RMSEs (in %).

Our results show that SVR and LSSVR have the potential to be an alternative to the DXA machine when measuring ALM and BMD.

Compared to the supervised regression algorithms we implemented in this paper, p -Laplacian based regression is not so well studied. In our analysis, p -Laplacian demonstrates that in the future, researchers could leverage using it, especially when training data is computationally or financially expensive. Like the supervised

models, both p -Laplacian-1 and p -Laplacian-2 perform considerably better for ALM and BMD compared to BFP. The errors are below 10% even when the training percent is significantly low. To predict BFP more accurately using p -Laplacian based regression, a higher correlated set of biomarkers with BFP could be used to construct the graph.

It is compelling to examine how the performance of the p -Laplacian model changes with the size of the dataset for a fixed proportion of training data. This way we can test if the number of data points in training impacts the model's performance differently than the proportion of training data.

Moreover, in our analysis, all the biomarkers are weighed equally to construct the similarity-based graph. Hence, one potential direction for future research is weighing the biomarkers differently. One such weighing could be based on how correlated they are with the target variable.

In summary, our results show DEXA could be potentially replaced in the future to estimate ALM and BMD. However, further investigation is needed on larger datasets. Additionally, our investigation of the p -Laplacian model yielded positive results for ALM and BMD in reducing the amount of training data while maintaining a high level of accuracy. Our analysis opens new avenues to implement and analyze the p -Laplacian model in regression problems.

10. Acknowledgements

We would like to thank the following people for their contribution to the early mathematical stages of the project: Gowri Priya Sunkara, Iswarya Sitiraju, Alex P Mensen-Johnson, Alyssa M Blount, Amaya Evans, Andrew Re-

gan, Anna S Crifasi, Artem Mukhamedzianov, Atif Iqbal, Berend P Grandt, David Aiken, Evan Short, Gaurang Chauhan, Giovanni Ohashiebula, Jamar K Whitfield, Kathyryn C Simon, Nuwanthi Samarawickrama, Serene Sam, Seth Stephens, Sunella A Ramnath, Teddie E Swize, Tristan Desoto, Joseph Dorta. We would like to thank Cassidy McCarty for her involvement with collecting the data.

This work was partially supported by National Science Foundation DMS grant 2407839 as well as by National Institutes of Health NORC Center Grants P30DK072476, Pennington/Louisiana, P30DK040561, Harvard; and R01DK109008, Shape UP! Adults. This work was also supported by the Bodin Undergraduate Summer Research Fund in the LSU Department of Mathematics.

References

- [1] Amina Adadi. A survey on data-efficient algorithms in big data era. *Journal of Big Data*, 8:24, 2021. doi: 10.1186/s40537-021-00419-9. URL <https://doi.org/10.1186/s40537-021-00419-9>.
- [2] Shara S.A. Alves, Elene F. Ohata, Navar M.M. Nascimento, João W. M. De Souza, Gabriel B. Holanda, Luiz Lannes Loureiro, and Pedro Pedrosa Rebouças Filho. Gender-based approach to estimate the human body fat percentage using machine learning. In *2021 International Joint Conference on Neural Networks (IJCNN)*, pages 1–8, 2021. doi: 10.1109/IJCNN52387.2021.9533512.
- [3] Mariette Awad and Rahul Khanna. *Support Vector Regression*, pages 67–80. Apress,

- Berkeley, CA, 2015. ISBN 978-1-4302-5990-9. doi: 10.1007/978-1-4302-5990-9_4. URL https://doi.org/10.1007/978-1-4302-5990-9_4.
- [4] S. Azadifar and A. Ahmadi. A novel candidate disease gene prioritization method using deep graph convolutional networks and semi-supervised learning. *BMC Bioinformatics*, 23(1):422, 2022. doi: 10.1186/s12859-022-04954-x. URL <https://doi.org/10.1186/s12859-022-04954-x>.
- [5] Thiago G. Barbosa-Silva, Maria Cristina Gonzalez, Renata M. Bielemann, Leonardo P. Santos, Caroline dos S. Costa, and Ana Maria B. Menezes. $2 + 2(+2) = 4$: A new approach for appendicular muscle mass assessment by ultrasound. *Nutrition*, 83:111056, 2021. ISSN 0899-9007. doi: <https://doi.org/10.1016/j.nut.2020.111056>. URL <https://www.sciencedirect.com/science/article/pii/S0899900720303397>.
- [6] J.P. Bennett, M.C. Wong, Y.E. Liu, B.K. Quon, N.N. Kelly, A.K. Garber, S.B. Heymsfield, and J.A. Shepherd. Trunk-to-leg volume and appendicular lean mass from a commercial 3-dimensional optical body scanner for disease risk identification. *Clinical Nutrition*, 43(10):2430–2437, October 2024. doi: 10.1016/j.clnu.2024.09.028. Epub 2024 Sep 16.
- [7] Céline Bentéjac, Adrien Csörgő, and Gustavo Martínez-Muñoz. A comparative analysis of gradient boosting algorithms. *Artificial Intelligence Review*, 54:1937–1967, 3 2021. doi: 10.1007/s10462-020-09896-5. URL <https://doi.org/10.1007/s10462-020-09896-5>. Published 24 August 2020.
- [8] Adam Bohr and Kaveh Memarzadeh. The rise of artificial intelligence in healthcare applications. In Adam Bohr and Kaveh Memarzadeh, editors, *Artificial Intelligence in Healthcare*, pages 25–60. Academic Press, 2020. doi: 10.1016/B978-0-12-818438-7.00002-2. Epub 2020 Jun 26. PMID: PMC7325854.
- [9] Jeff Calder. Graphlearning python package, January 2022. URL <https://doi.org/10.5281/zenodo.5850940>.
- [10] Jeff Calder and Nadejda Drenska. Consistency of semi-supervised learning, stochastic tug-of-war games, and the p-laplacian. *arXiv*, January 2024.
- [11] Jeff Calder and Nicolás García Trillos. Improved spectral convergence rates for graph laplacians on ϵ -graphs and k-nn graphs. *Applied and Computational Harmonic Analysis*, 60:123–175, 2022. ISSN 1063-5203. doi: <https://doi.org/10.1016/j.acha.2022.02.004>. URL <https://www.sciencedirect.com/science/article/pii/S1063520322000227>.
- [12] Jeff Calder, Dejan Slepčev, and Matthew Thorpe. Rates of convergence for laplacian semi-supervised learning with low labeling rates. *Research in the Mathematical Sciences*, 10(10), 2023. doi: 10.1007/s40687-022-00371-x. URL <https://doi.org/10.1007/s40687-022-00371-x>.
- [13] S.M. Nazia Fathima, R. Tamiselvi, and M. Parisa Beham. A survey on osteoporosis detection methods with a focus on x-ray and

- dexa images. *IETE Journal of Research*, 68 (6):4640–4664, 2022.
- [14] Robin Genuer and Jean-Michel Poggi. *Random Forests*, pages 33–55. Springer International Publishing, Cham, 2020.
- [15] Ian Goodfellow, Yoshua Bengio, and Aaron Courville. *Deep Learning*. MIT Press, 2016. <http://www.deeplearningbook.org>.
- [16] M. I. Higgins, J. P. Marquardt, V. A. Master, F. J. Fintelmann, and S. P. Psutka. Machine learning in body composition analysis. *European Urology Focus*, 7(4):713–716, Jul 2021. doi: 10.1016/j.euf.2021.03.013. Epub 2021 Mar 24. PMID: 33771476.
- [17] Andrew Jackson, Patricia Stanforth, Jean Gagnon, et al. The effect of sex, age and race on estimating percentage body fat from body mass index: The heritage family study. *International Journal of Obesity*, 26: 789–796, 2002. doi: 10.1038/sj.ijo.0802006.
- [18] Gareth James, Daniela Witten, Trevor Hastie, and Robert Tibshirani. *An Introduction to Statistical Learning: with Applications in R*. Springer, 2013. URL <https://faculty.marshall.usc.edu/gareth-james/ISL/>.
- [19] Gareth James, Daniela Witten, Trevor Hastie, Robert Tibshirani, and Jonathan Taylor. *An Introduction to Statistical Learning: with Applications in Python*. Springer, 2023. URL https://hastie.su.domains/ISLP/ISLP_website.pdf.download.html.
- [20] Ron Kohavi. A study of cross-validation and bootstrap for accuracy estimation and model selection. In *Proceedings of the 14th International Joint Conference on Artificial Intelligence*, 14:1137–1145, 03 2001.
- [21] Frederic Marazzato, Cassidy McCarthy, Ryan H Field, Han Nguyen, Thao Nguyen, John A Shepherd, Grant M Tinsley, and Steven B Heymsfield. Advances in digital anthropometric body composition assessment: neural network algorithm prediction of appendicular lean mass. *European Journal of Clinical Nutrition*, 78(5):452–454, 5 2024. doi: 10.1038/s41430-023-01396-3. Epub 2023 Dec 23.
- [22] N. Marin-Jimenez, C. Cruz-Leon, D. Sanchez-Oliva, J. Jimenez-Iglesias, I. Caraballo, C. Padilla-Moledo, et al. Criterion-related validity of field-based methods and equations for body composition estimation in adults: a systematic review. *Current Obesity Reports*, 11: 336–349, 2022.
- [23] C. McCarthy, G. M. Tinsley, S. Yang, B. A. Irving, M. C. Wong, J. P. Bennett, et al. Smartphone prediction of skeletal muscle mass: model development and validation in adults. *The American Journal of Clinical Nutrition*, 117:794–801, 2023.
- [24] Masakazu Shioji, Tetsuya Yamamoto, Takashi Ibata, Toshiyuki Tsuda, Keiichi Adachi, and Noriko Yoshimura. Artificial neural networks to predict future bone mineral density and bone loss rate in japanese postmenopausal women. *BMC Research Notes*, 10(1):590, 11 2017. doi: 10.1186/s13104-017-2910-4.
- [25] Sima Sobhiyeh, Samantha Kennedy, Alexander Dunkel, Marcelline E. Dechenaud, Jerome A. Weston, John

- Shepherd, Peter Wolenski, and Steven B. Heymsfield. Digital anthropometry for body circumference measurements: Toward the development of universal three-dimensional optical system analysis software. *Obesity Science & Practice*, 7(1):35–44, 2021. doi: <https://doi.org/10.1002/osp4.467>. URL <https://onlinelibrary.wiley.com/doi/abs/10.1002/osp4.467>.
- [26] Johan A.K. Suykens and Joos Vandewalle. Least squares support vector machine classifiers. *Neural Processing Letters*, 9(3):293–300, 1999. doi: 10.1023/A:1018628609742. URL <https://doi.org/10.1023/A:1018628609742>.
- [27] Mayooraan Thevaraja, Azizur Rahman, and Mathew Gabirial. Recent developments in data science: Comparing linear, ridge and lasso regressions techniques using wine data. In Faouzi Hidoussi, editor, *Proceedings of the International Conference on Digital Image & Signal Processing*, pages 1–6, United Kingdom, 04 . University of Oxford. URL <https://10times.com/disp-oxford>, <https://web.archive.org/web/20181203202733/https://www.disp-conference.org/>, <https://westminsterresearch.westminster.ac.uk/event/q9z0v/international-conference-on-digital-image-signal-processing-disp-19>.
- [28] H. Kalervo Väänänen and Pirkko L. Härkönen. Estrogen and bone metabolism. *Maturitas*, 23(Suppl):S65–S69, 1996. doi: 10.1016/0378-5122(96)01015-8.
- [29] Jesper E. van Engelen and Holger H. Hoos. A survey on semi-supervised learning. *Machine Learning*, 109:373 – 44a0, 2019. URL <https://api.semanticscholar.org/CorpusID:254738406>.
- [30] Yaqing Wang, Quanming Yao, James T. Kwok, and Lionel M. Ni. Generalizing from a few examples: A survey on few-shot learning. *ACM Computing Surveys (CSUR)*, 53(3):63:1–63:34, 2020. doi: 10.1145/3386252.
- [31] Qing Wu, Fatma Nasoz, Jongyun Jung, Bibek Bhattarai, Mira V. Han, Robert A. Greenes, and Kenneth G. Saag. Machine learning approaches for the prediction of bone mineral density by using genomic and phenotypic data of 5130 older men. *Scientific Reports*, 11(4482): 1–10, 2021. doi: <https://doi.org/10.1038/s41598-021-83828-3>.
- [32] Qiang Zeng, Sheng-Yong Dong, Xiao-Nan Sun, Jing Xie, and Yi Cui. Percent body fat is a better predictor of cardiovascular risk factors than body mass index. *Revista brasileira de pesquisas medicas e biologicas*, 45(7):591–600, 2012. doi: 10.1590/s0100-879x2012007500059.
- [33] Kang Zheng, Yirui Wang, Xiao-Yun Zhou, Fakai Wang, Le Lu, Chihung Lin, Lingyun Huang, Guotong Xie, Jing Xiao, Chang-Fu Kuo, and Shun Miao. Semi-supervised learning for bone mineral density estimation in hip x-ray images. In Marleen de Bruijne, Philippe C. Cattin, Stéphane Cotin, Nicolas Padoy, Stefanie Speidel, Yefeng Zheng, and Caroline Essert, editors, *Medical Image Computing and Computer Assisted Intervention – MICCAI 2021*, pages 33–42, Cham, 2021. Springer International Publishing.
- [34] Xiaojin Zhu. *Semi-Supervised Learning*

with Graphs. PhD thesis, Carnegie Mellon University, 2005.

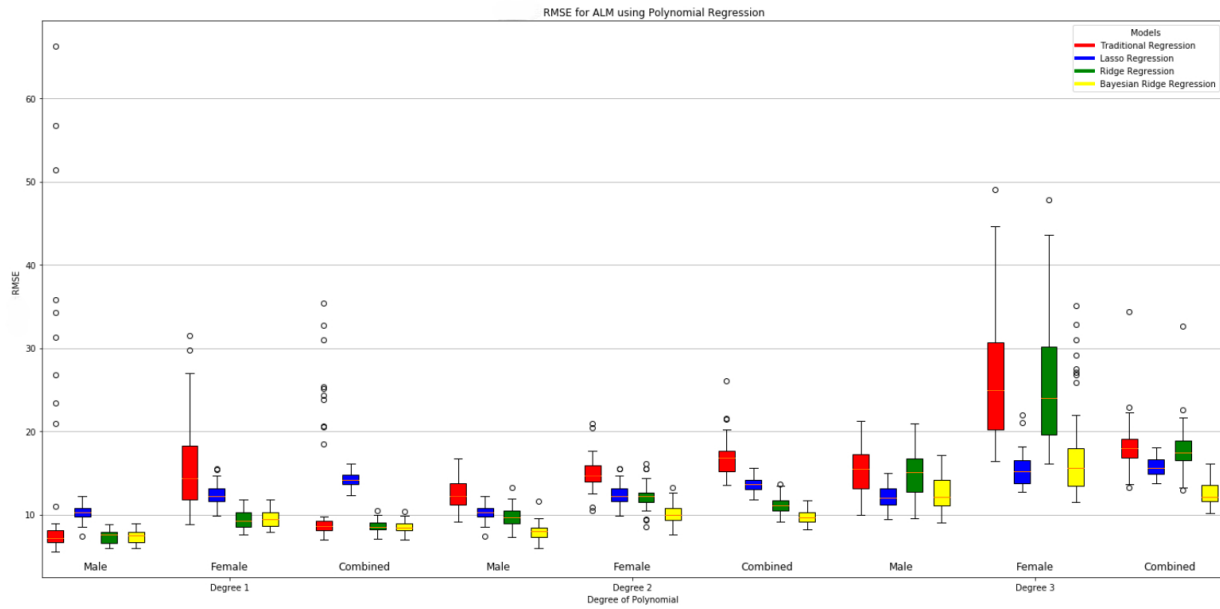


Figure 11: Distribution of RMSEs in predicting ALM by Polynomial Regression Models across Datasets

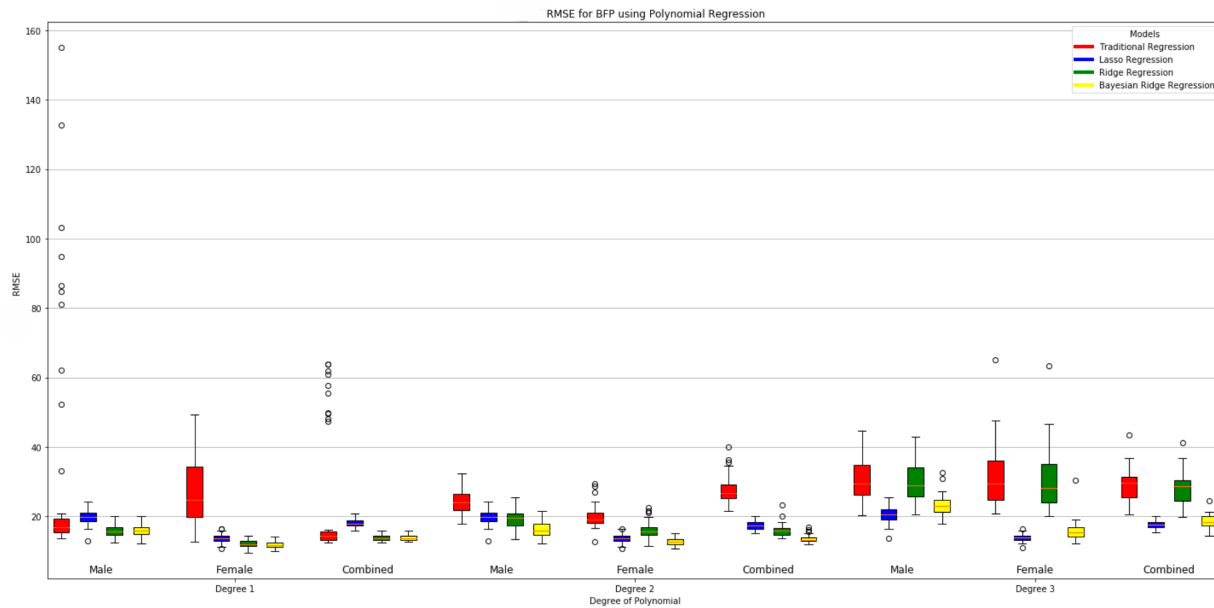


Figure 12: Distribution of RMSEs in predicting BFP by Polynomial Regression Models across Datasets

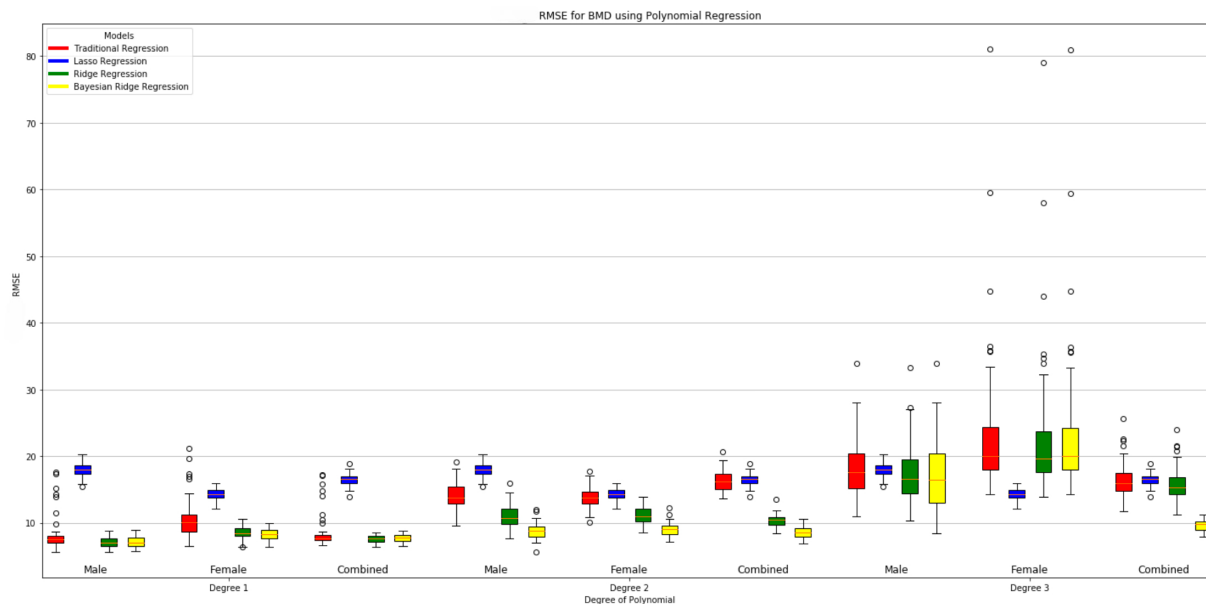


Figure 13: Distribution of RMSEs in predicting BMD by Polynomial Regression Models across Datasets

Height (cm)	Weight (kg)	Abdomen Circumference
Ankle Circumference Left	Arm Length Left	Arm Volume Left
Bicep Circumference Left	Calf Circumference Left	Chest
Collar Circumference	Forearm Circumference Left	Head Circumference
Hip Circumference	Horizontal Waist	Inseam Left
Leg Volume Left	MidThigh Circumference Left	Narrow Waist
Outside Leg Length Left	Seat Circumference	Surface Area Arm Left
Surface Area Leg Left	Surface Area Torso	Surface Area Total
Thigh Circumference Left	Torso Volume	Upper Arm Circumference Left
Volume	Waist Circumference	Ankle Circumference Right
Arm Length Right	Arm Volume Right	Bicep Circumference Right
Calf Circumference Right	Forearm Circumference Right	Inseam Right
Leg Volume Right	MidThigh Circumference Right	Outside Leg Length Right
Surface Area Arm Right	Surface Area Leg Right	Thigh Circumference Right
Upper Arm Circumference Right	Age	

Table 3: List of the Biomarkers

Male	Corr. Coeff.	Female	Corr. Coeff.	Combined	Corr. Coeff.
Surface Area Total	0.964	Surface Area Total	0.907	Surface Area Total	0.910
Surface Area Leg Right	0.956	Leg Volume Left	0.899	Surface Area Arm Left	0.904
Surface Area Leg Left	0.953	Surface Area Leg Right	0.898	Surface Area Arm Right	0.902
Surface Area Arm Left	0.947	Surface Area Leg Left	0.897	Weight (kg)	0.888
Leg Volume Left	0.944	Leg Volume Right	0.894	Surface Area Torso	0.875
Leg Volume Right	0.943	Weight (kg)	0.891	Forearm Circumference Right	0.872
Surface Area Arm Right	0.939	Volume	0.868	Surface Area Leg Right	0.869
Weight (kg)	0.934	Calf Circumference Left	0.865	Volume	0.865
Volume	0.922	Thigh Circumference Left	0.862	Surface Area Leg Left	0.865
Surface Area Torso	0.916	Thigh Circumference Right	0.861	Arm Volume Left	0.861

Table 4: Top 10 most correlated biomarkers with ALM with their Corresponding Correlation Coefficient

Male	Corr. Coeff.	Female	Corr. Coeff.	Combined	Corr. Coeff.
Horizontal Waist	0.577	Horizontal Waist	0.754	Waist Circumference	0.577
Narrow Waist	0.552	Waist Circumference	0.742	Horizontal Waist	0.566
Waist Circumference	0.526	Narrow Waist	0.741	Abdomen Circumference	0.559
Abdomen Circumference	0.512	Abdomen Circumference	0.741	Seat Circumference	0.510
Seat Circumference	0.444	Bicep Circumference Left	0.720	Hip Circumference	0.505
Hip Circumference	0.442	Chest	0.697	Thigh Circumference Left	0.479
Bicep Circumference Left	0.438	Upper Arm Circumference Right	0.691	Thigh Circumference Right	0.475
Torso Volume	0.436	Upper Arm Circumference Left	0.690	MidThigh Circumference Left	0.459
Chest	0.416	Bicep Circumference Right	0.688	MidThigh Circumference Right	0.448
Upper Arm Circumference Left	0.409	Torso Volume	0.665	Narrow Waist	0.442

Table 5: Top 10 most correlated biomarkers with BFP with their Corresponding Correlation Coefficient

Male	Corr. Coeff.	Female	Corr. Coeff.	Combined	Corr. Coeff.
Surface Area Arm Right	0.862	Height (cm)	0.733	Surface Area Total	0.806
Surface Area Arm Left	0.861	Surface Area Total	0.711	Height (cm)	0.804
Surface Area Total	0.851	Surface Area Leg Left	0.709	Surface Area Arm Left	0.795
Arm Volume Right	0.834	Surface Area Leg Right	0.696	Surface Area Arm Right	0.794
Height (cm)	0.834	Outside Leg Length Left	0.675	Surface Area Leg Left	0.782
Forearm Circumference Right	0.832	Outside Leg Length Right	0.662	Surface Area Leg Right	0.773
Arm Volume Left	0.831	Arm Length Left	0.659	Surface Area Torso	0.767
Surface Area Leg Left	0.829	Surface Area Torso	0.658	Arm Volume Right	0.765
Surface Area Leg Right	0.821	Surface Area Arm Left	0.654	Arm Volume Left	0.758
Surface Area Torso	0.816	Hip Circumference	0.652	Arm Length Left	0.749

Table 6: Top 10 most correlated biomarkers with BMD with their Corresponding Correlation Coefficient

p-Laplacian-1 (ALM)								
Dataset	Par./RMSE	80%	50%	33%	25%	20%	10%	5%
Male	p	2.0	5.5	8.5	10.0	10.0	10.0	10.0
	k	10	45	55	50	50	50	50
	RMSE	8.51	8.99	9.27	9.50	9.74	10.83	12.66
Female	p	3.5	4.5	5.0	5.5	6.5	7.5	9.5
	k	35	55	60	55	55	50	60
	RMSE	10.30	10.72	11.10	11.25	11.57	12.65	14.95
Combined	p	3.0	2.5	2.5	3.0	3.5	10.0	10.0
	k	15	10	10	10	10	20	35
	RMSE	9.97	10.46	11.05	11.42	11.84	13.21	15.20

Table 7: Optimal Parameters and Corresponding RMSEs of p -Laplacian-1 for ALM

p-Laplacian-1 (BFP)								
Dataset	Par./RMSE	80%	50%	33%	25%	20%	10%	5%
Male	p	3.0	2.5	3.0	3.5	10.0	10.0	10.0
	k	15	10	10	10	45	60	60
	RMSE	16.61	17.68	18.90	19.80	20.51	23.40	25.56
Female	p	3.0	3.0	4.0	4.5	5.0	6.0	8.0
	k	25	35	45	60	55	60	60
	RMSE	13.11	13.78	14.22	14.51	14.78	15.57	16.62
Combined	p	3.5	3.5	5.0	6.0	8.0	10.0	10.0
	k	15	15	15	15	15	15	15
	RMSE	14.62	15.50	16.46	17.10	17.68	19.92	22.19

Table 8: Optimal Parameters and Corresponding RMSEs of p -Laplacian-1 for BFP

p-Laplacian-1 (BMD)								
Dataset	Par./RMSE	80%	50%	33%	25%	20%	10%	5%
Male	p	2.5	3.0	3.0	3.0	3.5	4.5	9.5
	k	20	20	25	20	25	45	60
	RMSE	8.11	8.52	8.71	9.03	9.11	9.81	10.68
Female	p	2.0	2.0	2.0	2.5	2.5	2.5	7.0
	k	10	10	10	25	30	25	60
	RMSE	9.02	9.30	9.46	9.65	9.79	10.13	11.00
Combined	p	2.0	2.0	3.5	3.5	3.5	4.5	6.5
	k	15	15	40	40	45	50	55
	RMSE	8.57	8.86	9.06	9.19	9.34	9.65	10.23

Table 9: Optimal Parameters and Corresponding RMSEs of p -Laplacian-1 for BMD

p-Laplacian-2 (ALM)								
Dataset	Par./RMSE	80%	50%	33%	25%	20%	10%	5%
Male	p	2.0	2.0	2.5	3.0	3.0	3.0	3.5
	k	20	20	30	30	30	30	20
	RMSE	8.41	8.78	9.01	9.22	9.40	10.26	11.48
Female	p	2.5	2.5	2.5	2.5	2.5	3.0	4.0
	k	60	60	60	60	40	60	60
	RMSE	10.57	10.87	11.07	11.20	11.41	12.13	13.83
Combined	p	2.0	2.5	2.5	3.0	3.0	3.5	3.0
	k	20	25	25	30	30	60	40
	RMSE	11.69	12.11	12.56	12.79	13.02	13.64	14.72

Table 10: Optimal Parameters and Corresponding RMSEs of p -Laplacian-2 for ALM

p-Laplacian-2 (BFP)								
Dataset	Par./RMSE	80%	50%	33%	25%	20%	10%	5%
Male	p	2.0	2.0	2.5	2.5	4.5	2.0	2.0
	k	10	10	10	10	15	15	50
	RMSE	18.79	20.15	20.83	22.25	22.74	25.32	26.60
Female	p	2.5	2.5	2.5	2.0	2.5	2.0	2.0
	k	35	40	50	25	60	45	45
	RMSE	12.99	13.27	13.54	13.72	13.99	14.48	15.07
Combined	p	2.0	2.0	2.5	2.5	3.0	2.5	2.0
	k	15	15	20	25	50	60	60
	RMSE	20.94	21.59	22.54	22.92	23.30	24.43	25.10

Table 11: Optimal Parameters and Corresponding RMSEs of p -Laplacian-2 for BFP

p-Laplacian-2 (BMD)								
Dataset	Par./RMSE	80%	50%	33%	25%	20%	10%	5%
Male	p	2.0	2.0	2.0	2.0	2.0	2.0	2.5
	k	50	50	50	30	35	30	55
	RMSE	8.66	8.82	8.90	9.08	9.17	9.61	10.41
Female	p	2.5	2.0	2.0	2.0	2.0	2.0	2.5
	k	35	50	35	35	35	30	55
	RMSE	9.55	9.69	9.81	9.89	9.98	10.19	10.96
Combined	p	2.0	2.0	2.0	2.0	2.0	2.0	2.5
	k	55	50	45	45	45	45	55
	RMSE	9.11	9.22	9.34	9.39	9.47	9.63	10.09

Table 12: Optimal Parameters and Corresponding RMSEs of p -Laplacian-2 for BMD

Supervised Algorithms (ALM)				
Model	Par./RMSE	Male	Female	Combined
Regression	Par. RMSE	Traditional 8.00	Ridge 9.10	Bayesian 9.00
LSSVR	Par. RMSE	γ : 0.001, C : 500 7.47	γ : 0.001, C : 1000 6.03	γ : 0.001, C : 1000 8.46
NN	Par. RMSE	Epochs: 300 7.20	Epochs: 300 9.85	Epochs: 200 8.70
RF	Par. RMSE	n : 50, d : 15 7.96	n : 50, d : 15 10.52	n : 45, d : 25 10.06
SVR	Par. RMSE	ϵ : 0.7, C : 50 6.30	ϵ : 0.3, C : 1.0 8.97	ϵ : 0.4, C : 10 7.83
XGBoost	Par. RMSE	n : 35, d : 05 8.36	n : 35, d : 05 10.82	n : 35, d : 05 10.27

Table 13: Optimal Parameters and Corresponding RMSEs of Supervised Algorithms for ALM

Supervised Algorithms (BFP)				
Model	Par./RMSE	Male	Female	Combined
Regression	Par. RMSE	Ridge 18.00	Bayesian 14.60	Bayesian 17.00
LSSVR	Par. RMSE	γ : 0.01, C : 25 11.47	γ : 0.01, C : 25 12.09	γ : 0.001, C : 250 10.99
NN	Par. RMSE	Epochs: 300 14.20	Epochs: 400 12.00	Epochs: 250 12.80
RF	Par. RMSE	n : 50, d : 15 15.92	n : 50, d : 20 12.44	n : 50, d : 15 14.13
SVR	Par. RMSE	ϵ : 0.5, C : 0.7 14.92	ϵ : 1.0, C : 0.1 11.72	ϵ : 1.0, C : 1.0 13.28
XGBoost	Par. RMSE	n : 35, d : 05 16.40	n : 30, d : 05 12.89	n : 35, d : 05 14.55

Table 14: Optimal Parameters and Corresponding RMSEs of Supervised Algorithms for BFP

Supervised Algorithms (BMD)				
Model	Par./RMSE	Male	Female	Combined
Regression	Par. RMSE	Ridge 8.10	Bayesian 9.25	Ridge 8.00
LSSVR	Par. RMSE	γ : 0.001, C : 250 7.59	γ : 0.001, C : 100 7.05	γ : 0.01, C : 10 8.09
NN	Par. RMSE	Epochs: 200 7.35	Epochs: 350 8.60	Epochs: 400 7.90
RF	Par. RMSE	n : 45, d : 15 7.72	n : 50, d : 20 8.09	n : 50, d : 10 7.94
SVR	Par. RMSE	ϵ : 0.05, C : 0.2 6.97	ϵ : 0.05, C : 0.05 8.36	ϵ : 0.05, C : 0.4 7.48
XGBoost	Par. RMSE	n : 20, d : 05 8.22	n : 15, d : 05 8.37	n : 20, d : 05 8.31

Table 15: Optimal Parameters and Corresponding parameters of supervised algorithms for BMD